Crystallization of Antimony Nanoparticles: Pattern Formation and Fractal Growth[†]

Bert Stegemann,* Claudia Ritter, Bernhard Kaiser, and Klaus Rademann

Institut für Chemie, Humboldt-Universität zu Berlin, Brook-Taylor-Str. 2, D-12489 Berlin, Germany

Received: January 21, 2004; In Final Form: March 30, 2004

The spontaneous formation of complex interfacial patterns from thermally deposited Sb_4 clusters on HOPG is controlled by the deposition conditions (i.e., coverage and deposition rate) at constant temperature (300 K) under ultrahigh vacuum conditions. Two main driving forces for the pattern formation in this system have been identified. Initially, the crystallization of compact nanoparticles with spherical shape at a maximum diameter of 120 nm drives the system toward irregular, fingerlike shapes. Second, the ramification of these fingerlike nanoparticles is governed by the deposition rate, as the increase of the deposition rate allows the nanoparticle shape to be continuously tuned from fingerlike to further ramified and eventually fractal forms. On the basis of electron microscopy and atomic force microscopy measurements, these phenomena are quantified with a focus on fractal dimension, particle perimeter, and size of the side branches (tip width).

Introduction

The spontaneous formation of nanoscale patterns represents a powerful way to synthesize nanostructured materials.[1–3] The enormous interest in this field stems from both progress in fundamental research and advances in the miniaturization of electronic, optical, and mechanical components. Research is motivated by the prospect that the ability to control the building blocks of the nanostructures may result in enhanced material properties.[4–6] In this respect, clusters are very promising because of their fascinating size-dependent properties and huge efforts are directed toward the development of techniques for the assembly of size-selected clusters into nanostructured materials.[7–9] The self-organized growth of preformed clusters deposited from the gas phase has been accommodated as a practical design strategy for the growth of nanostructured systems.[10–12] In particular, diffusion, aggregation, and coalescence behavior of the clusters have been recognized to be the key points for the morphology of the emerging patterns. Their size, shape, and structure can be influenced by various experimental parameters during cluster deposition, such as the deposition rate (particle flux), the total amount deposited (coverage), or the substrate temperature. The study of how the morphology depends on the above-mentioned conditions contributes to the understanding of the fundamental growth mechanisms involved in pattern formation and, finally, leads to the control over the self-organized growth. Thus, the scope of this paper is to investigate how well-defined nanoscale pattern can be selectively grown, tuned, and modified through the control of the coverage and the deposition rate. We present a quantitative analysis of antimony nanoparticles spontaneously formed from monodisperse Sb_4 clusters on the (0001) surface of highly oriented pyrolitic graphite (HOPG) at room temperature.

Experimental Section

Sample preparation was performed in an ultrahigh vacuum (UHV) apparatus at a base pressure of less than 6×10^{-10} mbar.

Before deposition, clean HOPG(0001) surfaces were prepared by cleaving in air, immediately transferred into the UHV chamber, and heated for several hours at about 550 °C to remove atmospheric adsorbates. Antimony was deposited by thermal evaporation of the solid material (99.9999% purity) and condensation of the vapor onto the HOPG(0001) surface maintained at room temperature. Since exclusively Sb_4 clusters are present in the gas phase of antimony at temperatures of up to 830 K, only monodisperse clusters were deposited in this way.[13] As evaporation source, a custom-built Knudsen-like cell with a resistively heated crucible made of Shapal-M (Caburn-MDC Inc.) was employed. Shapal-M is a machinable ceramic with excellent thermal conductivity and an extremely low coefficient of thermal expansion. It ensures high-temperature stability of the source and thus the precise control of the deposition rate. The deposition rate can be varied over several orders of magnitude by adjusting the source temperature and is calibrated with a water-cooled crystal quartz microbalance, which can be placed at the position of the sample via a moveable bellow. For the experiments presented here, the deposition rate is varied from 1.0 to 20 Å/s, corresponding to particle fluxes of 0.8×10^{14} to 1.6×10^{15} $Sb_4/(s\cdot cm^2)$. Coverages are determined from deposition rate and time and will be scaled in equivalents of monolayers (ML), where 1 ML is defined as the nominal mass of antimony to form a layer of monatomic height (3.11 Å).

After deposition, the samples were transferred to air for subsequent surface analysis by scanning electron microscopy (SEM) with a Zeiss Gemini DS982 operated at 3–10 kV, by transmission electron microscopy (TEM) with a Hitachi H-8110 operated at 200 kV, and by atomic force microscopy (AFM) with a home-built instrument operated in the dynamic mode.[14] SEM was utilized for basic and convenient characterization of the surface morphology, whereas TEM and AFM were employed for disclosing detailed information on internal structure and three-dimensional shape of the nanoparticles. Since TEM is limited to thin samples being electron transparent, samples were prepared the following way: TEM copper grids were glued (Epo-Tek H21D, Caburn-MDC Inc.) onto the sample face and carefully peeled off, so that flakes of the top graphite layers

Crystallization of Antimony Nanoparticles
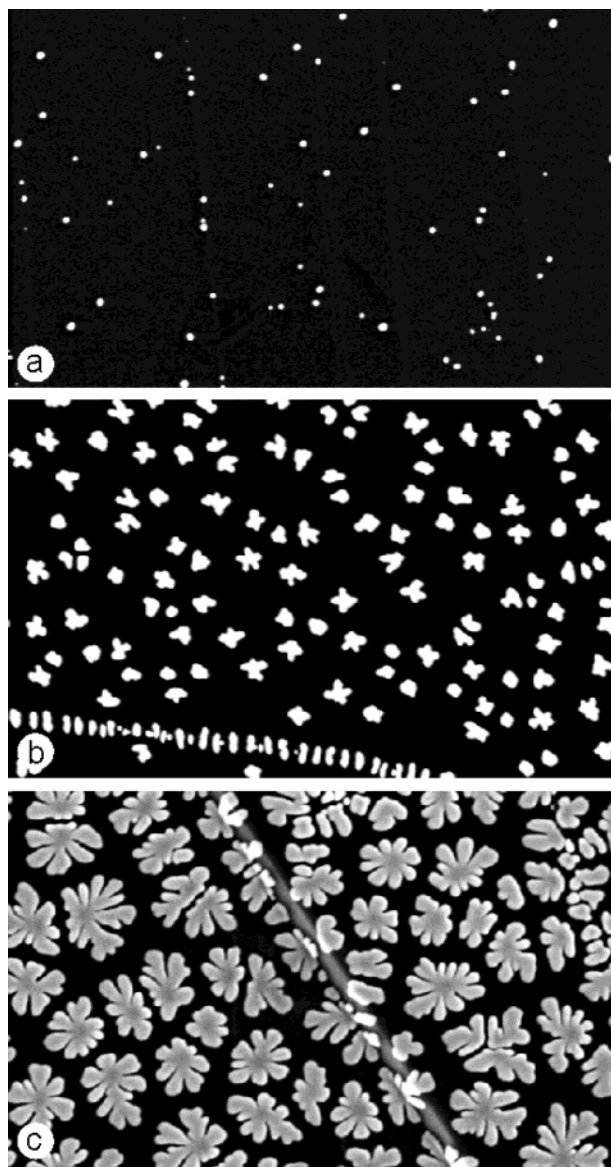
J. Phys. Chem. B, Vol. 108, No. 38, 2004 **14293**

Figure 1. SEM images (5.8 μm $\times$ 3.6 μm) of the surface morphology after deposition of (a) 2 ML, (b) 10 ML, and (c) 40 ML antimony on the HOPG(0001) surface at a deposition rate of 1.0 Å/s.

Figure 2. (a) TEM bright-field and (b) AFM image of typical spherical particles (cf. Figure 1a) at high magnification (500 nm $\times$ 500 nm). (c) Line scan as indicated in b.

Figure 3. (a) TEM bright-field and (b) AFM image of typical fingerlike particles (cf. Figure 1c) at high magnification (1000 nm $\times$ 1000 nm). (c) Line scan as indicated in b.

were torn off. It turned out that 100 mesh grids are best suited: (i) The grid bars (width 60 μm) provide a sufficiently large contact area to the surface. (ii) The open areas of the grid squares (180 μm) are not wetted by the glue and leave sufficient area that is available for surface imaging. If necessary, further thinning was achieved by peeling off graphite layers from the back.

Results and Discussion

Coverage Dependence. Typically, the bare HOPG(0001) cleavage plane exhibits large, atomically flat terraces with a lateral extension of up to a few square microns. Sb$_4$ clusters deposited thermally onto the room-temperature HOPG(0001) surface are very mobile because of the weak interaction between the clusters and the graphite. Therefore, they tend to form three-dimensional nanoparticles according to the Volmer–Weber-type growth mode. The SEM images in Figure 1 show the typical surface morphologies for three different coverages. At low antimony coverages (2 ML), exclusively compact nanoparticles of spherical shape are formed (Figure 1a), whereas at an
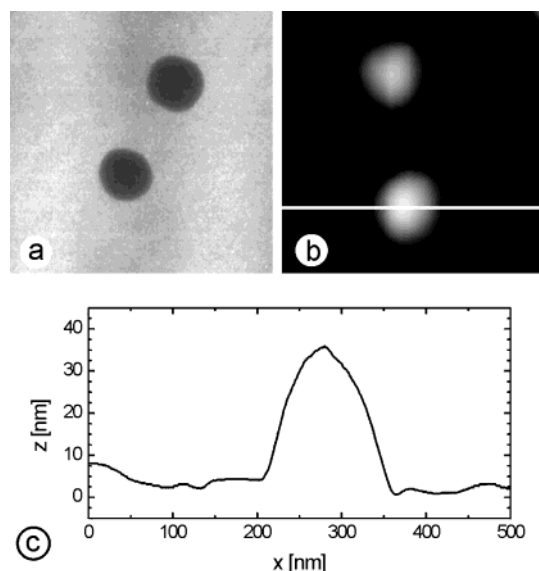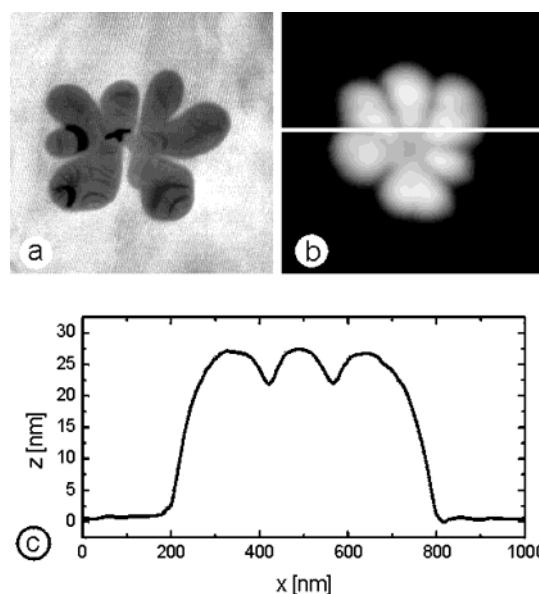
intermediate coverage of 10 ML, the particles exhibit a rather irregular shape (Figure 1b). Eventually, at the highest coverage shown (40 ML) predominantly fingerlike particle shapes are observed (Figure 1c). In previous work it has been shown that the spherical particles grow by incorporating encountered Sb$_4$ clusters and retain their spherical shape until they reach a diameter of about 120 nm and that further deposition leads to a transition from spherical to fingerlike particle shapes.[15]

To obtain deeper insights into this morphological transition, detailed information on the basic particle shapes—spherical and fingerlike—are extracted from TEM and AFM analysis. These two techniques allow to obtain complementary information, as TEM measurements give the precise projected diameter and AFM measurements provide the exact height of the supported particle. The micrographs presented in Figures 2 and 3 demonstrate that in principle the morphologies imaged by AFM are consistent to those in the TEM image, when a convolution of surface topography and tip shape in the AFM image is taken

into account. Figure 2 provides enlarged views of alike surface regions of the sample presented in Figure 1a acquired by bright-field TEM (Figure 2a) and by AFM (Figure 2b). A height profile across a spherical particle as indicated by the line in the AFM image is given in Figure 2c. The three-dimensional character is clearly verified. The mean diameter of a large number of such particles has been measured to be 110 ± 10 nm. Spherical particles with a mean diameter of more than 120 nm have never been observed.[15] The characteristic height is about 35 nm, resulting in an aspect ratio (=height/lateral diameter) of nearly 1/3. This value has been quantitatively confirmed for particles of different size. A TEM and an AFM image of fingerlike particles which are considered to be representative for the entire ensemble at a total coverage of 40 ML (cf. Figure 1b) are provided in Figure 3. The lateral diameter of these particles is typically in the range of 500−700 nm and the height is measured to be about 25 nm. Additional information can be deduced from the TEM images in Figures 2a and 3a. In Figure 2a, the spherical particles exhibit a rather homogeneous dark color, which has been interpreted as scattering contrast arising from variations in mass and thickness. Mass−thickness contrast is considered to be the main contrast mechanism for noncrystalline specimen.[16] Moreover, investigations of the spherical particles by selected area diffraction and convergent beam diffraction did not show any indication of crystalline properties. Thus, it is confirmed that the spherical particles are not crystalline at all. In contrast, the fingerlike particles clearly produce dark contour lines in the bright-field TEM image (cf. Figure 3a). These patterns are unequivocally identified as bending contours, since their particular positions move when the sample is tilted. In TEM, bending contours clearly indicate the existence of a crystal lattice, because they only occur when a particular set of diffracting lattice planes is not parallel.[17] As a consequence, the fingerlike particles are considered to be crystalline with some degree of internal strain. It can be concluded that the morphological transition from spherical to fingerlike particle shapes is associated with a phase transition from amorphous to crystalline.

To account for these observations, the following scenario is proposed: In the initial stage of growth, nanoparticles are spontaneously formed by aggregation and coalescence of diffusing Sb_4 clusters. These nanoparticles tend to reduce the total amount of surface by adopting a spherical shape. This kind of compact particle shape is obtained, if the coalescence time is shorter than the time interval between successive arrivals of clusters to the nanoparticle.[18,19] In the course of growth, the nanoparticles transform continuously their shape when an Sb_4 cluster is encountered to retain their spherical shape. At coverages of less than 4 ML, this behavior is irrespective of the deposition rate. In this growth regime, the particles do not build up any crystalline order and no facets are formed, as documented in Figures 1a and 2. The experiments have shown that at a maximum diameter of 120 nm the spherical morphology is not stable anymore and the nanoparticles spontaneously crystallize and form irregular shapes. This shape relaxation results in fingerlike particles which are flattened in comparison to the spherical particles but reach larger lateral extensions. This morphology transition is driven by the crystallization. It can be understood as result of the interplay of thermodynamic and kinetic processes: the formation of crystalline order according to the equilibrium crystal symmetry and on the other hand the formation of side branches with a large surface area to facilitate the efficient removal of the latent heat generated during crystallization. The prevailing strain in the fingerlike particles indicates a rapid crystallization.[20] As the cluster deposition is
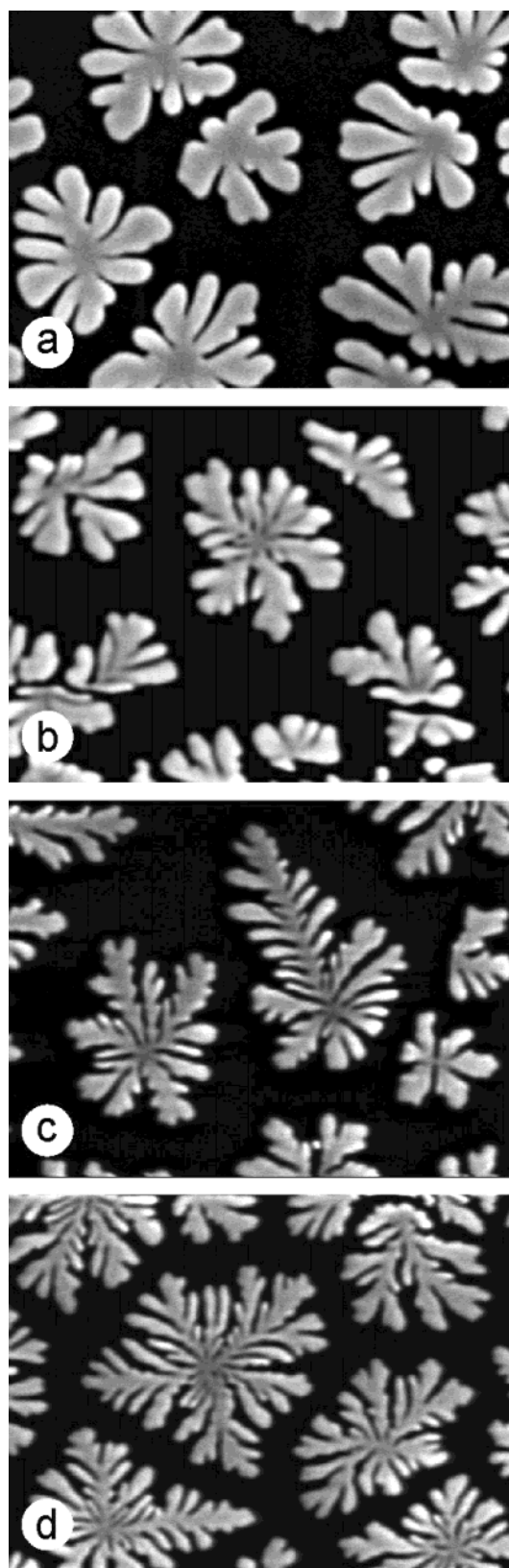

Figure 4. SEM images (2.2 μm $\times$ 1.6 μm) of the evolution of the surface morphology after deposition of 40 ML antimony at deposition rates of (a) 1.0 Å/s, (b) 2.0 Å/s, (c) 10 Å/s, and (d) 20 Å/s.

continued, the side branches grow radially outward by capture of diffusing Sb_4 clusters, leading to fingerlike particle shapes as seen Figures 1c and 3.

Deposition Rate Dependence. Figure 4 shows a series of SEM images of the surface morphology at different deposition

Crystallization of Antimony Nanoparticles

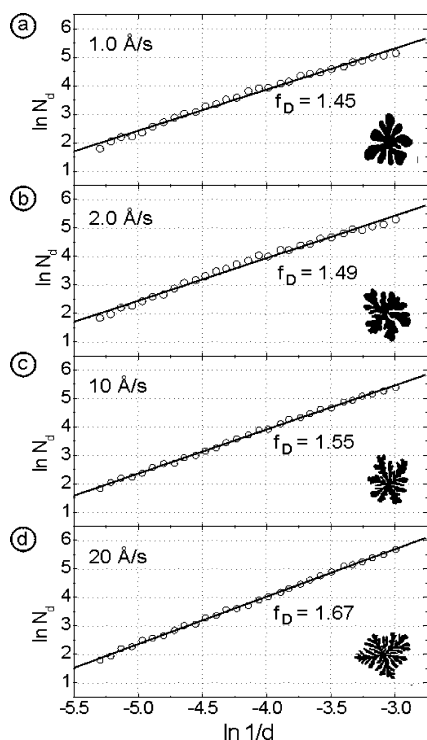*J. Phys. Chem. B, Vol. 108, No. 38, 2004* **14295**

Figure 5. Fractal analysis of the featured nanoparticles obtained at a deposition rate of (a) 1.0 Å/s, (b) 2.0 Å/s, (c) 10 Å/s, and (d) 20 Å/s. The graphs display the number of boxes N_d needed to cover the particle as a function of the inverse box size d. The slope yields the fractal dimension f_D.

Figure 6. Quantitative analysis of the featured particles at different deposition rates: (a) fractal dimension f_D, (b) ratio of perimeter P and square root of the area of the particle projection A_p, (c) mean width of the outer tip ends w_{tip}.

rates and a constant coverage of 40 ML. These images reveal the evolution of the nanoparticle shape, when the deposition rate is increased from 1.0 Å/s (Figure 4a) to 20 Å/s (Figure 4d). The increase of the deposition rate leads to a distinct increase of the particle ramification without significant change of the island density.

A useful quantity for the characterization of such complex growth patterns and for establishing a relationship to experimental parameters is the fractal dimension f_D. Several methods have been developed to estimate f_D. In this respect, the box-counting method has been proven to be of sufficient accuracy and efficiency.[21] This method works by covering the object with a grid of square boxes of size d and counting the number of boxes N_d needed for complete coverage. If the object is fractal, a linear fit to the logarithmic plot of N_d versus $1/d$ yields the fractal dimension (box dimension). To analyze the fractal properties of the morphologies shown in Figure 4, a prototype of each of the four samples has been selected, which is considered to be representative in shape and size for the entire ensemble and apparently not influenced by surface irregularities, such as step edges. The fractal analysis of the digitized images of these particles is presented in Figure 5. For all four particles, the data points are on a straight line and the fractal dimension can be estimated from the slope. A value of $f_D = 1.45$ for the most compact particle (Figure 5a) and of $f_D = 1.67$ for the most ramified particle (Figure 5d) is found. Extrapolating this trend to more ramified nanoparticles, f_D is expected to approach the value of 1.71, which is the fractal dimension of a particle obtained by simulation of diffusion-limited-aggregation (DLA).[22] Figure 6a summarizes the results of the fractal analysis in detail. The increasing ramification is corroborated by the analysis of further accessible parameters characterizing the selected nanoparticles. In Figure 6b, the perimeters, that is, the contour lengths of the projections of the investigated particles, are displayed.
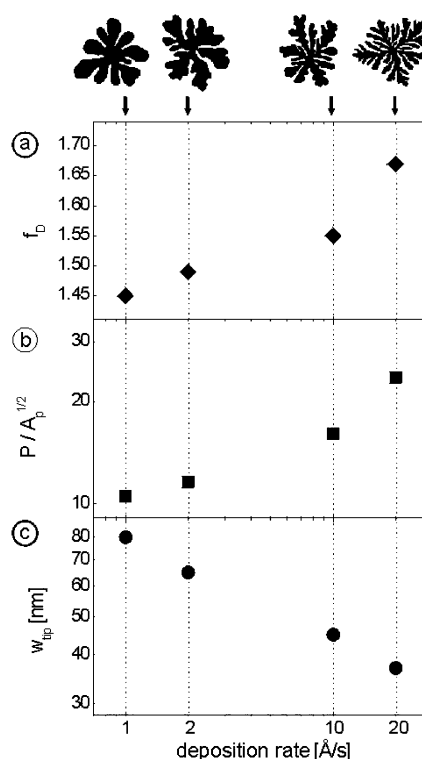
For comparison, these values are normalized by the projected particle area. A distinct increase of the perimeter on changing the deposition rate to higher values is found. Figure 6c shows that the mean tip width of the outer ends of the side branches (determined at the center of the radius of curvature) decreases with increasing ramification.

The correlation between the shapes of the antimony nanoparticles and the experimental conditions exhibits a striking resemblance to many systems in nature. It has been recognized that a wide variety of patterns is controlled by the strength of a gradient of a field at the interface.[21,23,24] For example, the growth rate in electrochemical deposition depends on the gradient of the applied voltage, in viscous fingering it depends on the pressure gradient, in solidification it depends on the temperature gradient, and in aggregation processes it is proportional to the concentration of the diffusing particles. All these processes have in common that they are described by the diffusion equation, which is approximated in the steady state by the Laplacian equation: $\Delta u = 0$. In this equation, the field u may denote the controlling field, that is, the voltage, pressure, temperature, or concentration. Variations in the boundary conditions imposed on u are reflected by differences in the resulting morphologies. As shown in electrochemical deposition experiments, the morphology of the metal deposit depends on the controlling field as follows: At low electrical voltages, smooth metal films are formed, whereas high voltages give rise to fractal patterns.[25] Another common example is the formation of viscous fingers when a less viscous fluid is injected into a more viscous one. In this case, on increasing the pressure the resulting pattern is modified from fingerlike to dendritic and eventually to highly branched structures.[26]

It turned out that all these morphologies in different physical contexts can effectively be reproduced by the DLA model.[21,24] In the DLA model, diffusing particles that come into contact

Figure 7. SEM image (3.75 μm $\times$ 2.4 μm) of nanoparticles with sixfold symmetry formed at a deposition rate of 2.0 Å/s and a coverage of 55 ML.

with a growing aggregate stick in the position at which they arrived first.[22] The aggregates generated by this process are highly ramified and their fractal structure arises because the fast-growing outer parts shield the inner parts which are less accessible for incoming particles. Pure DLA growth leads to branches with a width of exactly the size of the precursor particle. Fractals with wider branches, such as in viscous fingering, were simulated by incorporating surface tension and surface diffusion. These simulations led to fractal dimensions in the range of 1.45 and 1.50 and pointed out the universality of DLA.[24,27]

The morphologies of the antimony nanoparticles resemble those simulations of DLA patterns in the following respects: (i) Driving force and hence the controlling field for the increasing ramification is the concentration of diffusing Sb_4 clusters. This concentration is correlated to the deposition rate and therefore to the flux of Sb_4 clusters that is incident on the surface: the faster the deposition rate, the shorter the time interval between successive captures of Sb_4 clusters by an existing aggregate and the faster the growth at a certain point on the interface. In accordance to, for example, viscous fingering, the increase of the driving force allows the resulting pattern to be tuned from fingerlike to more ramified structures. (ii) The branch widths, which are much larger than the size of the incident Sb_4 clusters, and the fractal dimensions in the range from 1.45−1.67 imply that in our system surface tension and surface diffusion of Sb_4 clusters at the interface are inherent. The activation energy for the diffusion of an Sb_4 along the periphery of a larger aggregate is 700 meV,[28] which is approximately 1 order of magnitude higher than the value of 60 meV for surface diffusion of Sb_4 on HOPG(0001).[29] This high activation barrier possibly accounts for the observed morphologies (cf. Figure 4) that resemble simulations of DLA growth with surface tension, as it counteracts complete coalescence, but still prevents branching at small scales. (iii) In several cases, it appears that the nanoparticles exhibit a rather dendritic character than being completely random. An accumulation of such oriented particles with sixfold symmetry encountered at a deposition rate of 2.0 Å/s is shown in Figure 7. As the interaction between the deposit and the HOPG substrate is very weak, the orientation of the branches of these aggregates can be correlated well with the hexagonal orientation of bulk antimony[30] and indicates a (0001) termination of the nanoparticles.[31] Thus, in particular at intermediate deposition rates (2.0 Å/s) the crystallographic orientation introduces an effective anisotropy to the fractal growth. Again, this effect agrees well with the formation of dendritic pattern at intermediate driving forces as observed

in viscous fingering. These results clearly show that the experimental growth patterns possess general features and are qualitatively and quantitatively in accord with those generated from simulations of DLA.

Conclusions

Various complex interfacial patterns are selectively grown by thermal deposition of Sb_4 clusters onto the HOPG(0001) surface kept at room temperature and characterized by means of SEM, TEM, and AFM. It is demonstrated that precise control of the experimental conditions, that is, coverage and deposition rate, allows the tuning and modification of the emerging patterns.

In the early stages of growth, the morphology is mainly dependent on the coverage, irrespective of the deposition rate. At low coverage (2 ML), compact particles with spherical shape are formed, which reach a maximum lateral diameter of 120 nm at an aspect ratio of about 1/3. When the coverage is increased, a complete morphology change from spherical to fingerlike particles sets in, driven by a rapid phase transition from amorphous to crystalline. This morphology change reflects a competition between order associated with the crystal symmetry and disorder related to the formation of a large amount of surface area for facile transfer of latent heat. Continued deposition leads to a branched outward growth of the fingerlike particles by capture of Sb_4 clusters. This fingerlike morphology emerges because of screening effects of the outer branches and diffusion of Sb_4 clusters along the surface of the nanoparticle. At this stage of growth, the ramification of these nanoparticles is strongly dependent on the deposition rate. In particular, on increasing the deposition rate from 1.0 to 20 Å/s the shape of the fingerlike nanoparticles can be tuned from fingerlike to more ramified and fractal forms. The differences in the obtained fractal morphologies have been quantitatively analyzed in terms of fractal dimension, contour length, and tip width.

In conclusion, the phase transition and, subsequently, the deposition rate act as driving forces for the pattern formation in the system antimony on HOPG(0001). Moreover, the observed patterns are of striking resemblance to many patterns observed in a variety of systems, which are controlled by the strength of a field gradient at the interface and which can be simulated by DLA.

References and Notes

(1) Ertl, G. *Electrochim. Acta* **1998**, *43*, 2743−2750.

(2) Gollub, J. P.; Langer, J. S. *Rev. Mod. Phys.* **1999**, *71*, S396−S403.

(3) Xia, Y.; Rogers, J. A.; Paul, K. E.; Whitesides, G. M. *Chem. Rev.* **1999**, *99*, 1823−1848.

(4) *Metal Clusters at Surfaces: Structure, Quantum Properties, Physical Chemistry*; Meiwes-Broer, K.-H., Ed.; Springer: Berlin, 2000.

(5) Moriarty, P. *Rep. Prog. Phys.* **2001**, *64*, 297−381.

(6) Freund, H.-J. *Surf. Sci.* **2002**, *500*, 271−299.

(7) Kreibig, U.; Bönnemann, H.; Hornes, J. In *Handbook of Surfaces and Interfaces of Materials*; Nalwa, H. S., Ed.; Academic Press: San Diego, 2001; Vol. 3, pp 1−87.

(8) Binns, C. *Surf. Sci. Rep.* **2001**, *44*, 1−49.

(9) Eberhardt, W. *Surf. Sci.* **2002**, *500*, 242−270.

(10) Jensen, P. *Rev. Mod. Phys.* **1999**, *71*, 1695−1735.

(11) Brechignac, C.; Cahuzac, P.; Carlier, F.; Defrutos, M.; Masson, A.; Mory, C.; Colliex, C.; Yoon, B. *Phys. Rev. B* **1998**, *57*, R2084−R2087.

Crystallization of Antimony Nanoparticles

J. Phys. Chem. B, Vol. 108, No. 38, 2004 **14297**

(12) Kaiser, B.; Stegemann, B. *ChemPhysChem* **2004**, *5*, 37−42.

(13) Mühlbach, J.; Pfau, P.; Recknagel, E.; Sattler, K. *Surf. Sci.* **1981**, *106*, 18−26.

(14) Ritter, C.; Heyde, M.; Schwarz, U. D.; Rademann, K. *Langmuir* **2002**, *18*, 7798−7803.

(15) Kaiser, B.; Stegemann, B.; Kaukel, H.; Rademann, K. *Surf. Sci.* **2002**, *496*, L18-L22.

(16) *Characterization of Nanophase Materials*; Wang, Z. L., Ed.; Wiley-VCH: Weinheim, 2000.

(17) Williams, D. B.; Carter, C. B. *Transmission Electron Microscopy*; Plenum Press: New York, 1996.

(18) Yoon, B.; Akulin, V. M.; Cahuzac, P.; Carlier, F.; de Frutos, M.; Masson, A.; Mory, C.; Colliex, C.; Brechignac, C. *Surf. Sci.* **1999**, *443*, 76−88.

(19) Brechignac, C.; Cahuzac, P.; Carlier, F.; Colliex, C.; de Frutos, M.; Kebaili, N.; Le Roux, J.; Mason, A.; Yoon, B. *Eur. Phys. J. D* **2001**, *16*, 265−269.

(20) Langer, J. S. *Rev. Mod. Phys.* **1980**, *52*, 1−28.

(21) Barabasi, A. L.; Stanley, H. E. *Fractal Concepts in Surface Growth*; University Press: Cambridge, UK, 1995.

(22) Witten, T. A.; Sander, L. M. *Phys. Rev. Lett.* **1981**, *47*, 1400−1403.

(23) Family, F. In *Computer Simulation Studies in Condensed Matter Physics*; Landau, D. P., Moon, K. K., Schüttler, H. B., Eds.; Springer: Berlin, 1988; pp 65−75.

(24) Meakin, P. *Fractals, scaling and growth far from equilibrium*; University Press: Cambrige, UK, 1998.

(25) Ben-Jacob, E.; Garik, P. *Nature* **1990**, *343*, 523−530.

(26) *Pattern Formation in Liquid Crystals*; 2nd ed.; Buka, A., Kramer, L., Eds.; Springer: New York, 1996.

(27) Meakin, P. *Phys. Rev. Lett.* **1983**, *51*, 1119−1122.

(28) Bardotti, L.; Jensen, P.; Hoareau, A.; Treilleux, M.; Cabaud, B.; Perez, A.; Aires, F. S. *Surf. Sci.* **1996**, *367*, 276−292.

(29) Stegemann, B.; Opitz, J.; Kaiser, B.; Rademann, K. In *Cluster and Nanostructure Interfaces*; Jena, P., Khanna, S. N., Rao, B. K., Eds.; World Scientific: Singapore, 2000; pp 601−606.

(30) Stegemann, B.; Ritter, C.; Kaiser, B.; Rademann, K. *Phys. Rev. B* **2004**, *69*, 155432.

(31) Savage, D. E.; Lagally, M. G. *Appl. Phys. Lett.* **1987**, *50*, 1719−1721.